

# Efficient and robust constitutive integrators for single-crystal plasticity modeling

S.N. Kuchnicki<sup>1</sup>, A.M. Cuitiño<sup>1</sup>, R.A. Radovitzky<sup>2</sup>

<sup>1</sup>Department of Mechanical and Aerospace Engineering,  
Rutgers University, Piscataway, NJ 08854 USA

<sup>2</sup>Department of Aeronautics and Astronautics,  
Massachusetts Institute of Technology  
Cambridge, MA 02139 USA

## Abstract

Small-scale deformation phenomena such as subgrain formation, development of texture, and grain boundary sliding require simulations with a high degree of spatial resolution. When we consider finite-element simulation of metal deformation, this equates to thousands or hundreds of thousands of finite elements. Simulations of the dynamic deformations of metal samples require elastic-plastic constitutive updates of the material behavior to be performed over a small time step between updates, as dictated by the Courant condition. Further, numerical integration of physically-based equations is inherently sensitive to the step in time taken; they return different predictions as the time step is reduced, eventually approaching a stationary solution. Depending on the deformation conditions, this converged time step becomes short ( $10^{-9}$  s or less). If an implicit constitutive update is applied to this class of simulation, the benefit of the implicit update (i.e., the ability to evaluate over a relatively large time step) is negated, and the integration is prohibitively slow. The present work recasts an implicit update algorithm into an explicit form, for which each update step is five to six times faster, and the compute time required for a plastic update approaches that needed for a fully-elastic update. For dynamic loading conditions, the explicit model is found to perform an entire simulation up to 50 times faster than the implicit model. The performance of the explicit model is enhanced by adding a subcycling algorithm to the explicit model, by which the maximum time step between constitutive updates is increased an order of magnitude. These model improvements do not significantly change the predictions of the model from the implicit form, and provide overall computation times significantly faster than the implicit form over finite-element meshes. These modifications are also applied to polycrystals via Taylor averaging, where we also see improved model performance.

# 1 Introduction

The explosion in computing power over the last few decades has heightened the aspirations of numerical analysts. Simulations previously thought difficult are now commonplace; those once considered impossible or impractical are now merely time-consuming. Increased computing power has seen an additional focus on the behavior of polycrystalline metals, of both face-centered cubic and body-centered cubic crystal structure.

The basis for modern crystal plasticity is modeling of single crystals. Averaging techniques for polycrystals rely upon a well-formulated representation of the single crystal. Alternately, direct numerical simulation of polycrystals [31] models a particular multi-crystalline material by tracking the interactions between several single crystals. Both of these methods for capturing the behavior of polycrystals are computationally intensive; the goal of the modeler at the constitutive level is thus to provide the fastest model possible while retaining the underlying physics of the model (and, by extension, the model accuracy).

The fundamental importance of single crystal modeling is reflected in the abundance of theories on monocrystalline plasticity in the literature. Such theories begin to appear in the literature in the early 20<sup>th</sup> century and are presented by many investigators, including: Taylor [29], [28]; Schmid [27]; Bishop [4]; Hill [12]; Rice [26]; Hutchinson [13]; Asaro [2], [1]; Havner [10], [11]; Bassani [3]; and Kocks [14]. We seek neither to provide a comprehensive review of these theories, nor do we wish to provide a comparison among them. Rather, we will use the update procedure of Cuitiño and Ortiz [5], first in an implicit form as originally presented. In the interest of increasing the computational speed of the model, we will present an explicit form of this model. Then, in view of the relatively short time steps allowed by the explicit integration, we arrive at a convergence condition for the explicit integration. Using this condition, we are able to devise a subcycling scheme that allows the explicit integration to converge over larger user-specified time steps. We illustrate these model improvements with numerical examples, which include the computation time required for each.

# 2 Constitutive Framework

As stated earlier, we are applying the model of Cuitiño and Ortiz [5] for our work here. We briefly review the fundamentals of this model here in order to make the current work as self-contained as possible.

Our current model follows the lead of numerous previous authors, including but not limited to Lee [17], [16]; Kratochvil [15]; Green and Naghdi [9]; Mandel [20]; Nemat-Nasser [22]; Onat [23]; Loret [19]; and Dafalias [6]. The underlying assumption common to all these theories is that the overall deformation gradient  $\mathbf{F}$  can be decomposed into an elastic component  $\mathbf{F}^e$  and a plastic part  $\mathbf{F}^p$ , as:

$$\mathbf{F} = \mathbf{F}^e \mathbf{F}^p \tag{1}$$

The existence of such a multiplicative decomposition implies that there is

some stress-free intermediate configuration which contains the deformation due to plastic slip only; lattice distortion and rotation are presumed to be contained in  $\mathbf{F}^e$ . The plastic deformation gradient is assumed to be volume-conserving. These assumptions ensure that the decomposition (1) is unique. The deformation power per unit undeformed volume can thus be written

$$\mathbf{P} : \dot{\mathbf{F}} = \bar{\mathbf{P}} : \dot{\mathbf{F}}^e + \bar{\boldsymbol{\Sigma}} : \bar{\mathbf{L}}^p \quad (2)$$

where  $\bar{\mathbf{P}} = \mathbf{P}\mathbf{F}^{pT}$  is a first Piola-Kirchhoff stress tensor relative to the intermediate configuration, and  $\bar{\boldsymbol{\Sigma}} = \mathbf{F}^{eT}\mathbf{P}\mathbf{F}^{pT}$  is a stress measure conjugate to the plastic velocity gradients on the intermediate configuration, given by  $\bar{\mathbf{L}}^p = \dot{\mathbf{F}}^p\mathbf{F}^{pT}$ . The work conjugacy relations (2) imply forms for the plastic flow rule and elastic stress-strain relations, i.e.,

$$\begin{aligned} \bar{\mathbf{L}}^p &= \bar{\mathbf{L}}^p(\bar{\boldsymbol{\Sigma}}, \bar{\mathbf{Q}}) \\ \bar{\mathbf{P}} &= \bar{\mathbf{P}}(\mathbf{F}^e, \bar{\mathbf{Q}}) \end{aligned} \quad (3)$$

where  $\bar{\mathbf{Q}}$  represents the appropriate internal variables defined on the intermediate configuration, subject to appropriate evolution equations (hardening laws). The most general form of the second of (3) that is material-frame indifferent is

$$\bar{\mathbf{P}} = \mathbf{F}^e \bar{\mathbf{S}}(\bar{\mathbf{C}}^e) \quad (4)$$

where  $\bar{\mathbf{C}}^e = \mathbf{F}^{eT}\mathbf{F}^e$  is the right Cauchy-Green deformation tensor on the intermediate configuration, and  $\bar{\mathbf{S}} = \bar{\mathbf{C}}^{e-1}\bar{\boldsymbol{\Sigma}}$  is a symmetric second Piola-Kirchhoff stress tensor on the intermediate configuration. For metals, we can assume a linear relation between  $\bar{\mathbf{S}}$  and the elastic Lagrangian strain on the intermediate configuration,  $\bar{\mathbf{E}}^e = (\bar{\mathbf{C}}^e - \mathbf{I})/2$  without loss of generality. Higher-order moduli are available, for example, see Teodosiu [30].

Rice [26] has shown that the formulation of  $\bar{\mathbf{L}}^p$  used here has the structure

$$\bar{\mathbf{L}}^p = \sum_{\alpha} \dot{\gamma}^{\alpha} \bar{\mathbf{s}}^{\alpha} \otimes \bar{\mathbf{m}}^{\alpha} \quad (5)$$

where  $\dot{\gamma}^{\alpha}$  is the shear rate on slip system  $\alpha$ , which has slip direction  $\bar{\mathbf{s}}^{\alpha}$  and normal vector  $\bar{\mathbf{m}}^{\alpha}$ . We follow the usual assumption that these slip rates depend on stress through the corresponding resolved shear stress  $\tau^{\alpha}$  only, meaning

$$\dot{\gamma}^{\alpha} = \dot{\gamma}^{\alpha}(\tau^{\alpha}, \bar{\mathbf{Q}}) \quad (6)$$

Peirce, *et al* [25] and several others have proposed a power law representation for the slip rates,

$$\dot{\gamma}^{\alpha} = \begin{cases} \dot{\gamma}_0 \left( \frac{\tau^{\alpha}}{g^{\alpha}} \right)^{\frac{1}{m}}, & \tau^{\alpha} \geq 0 \\ 0, & \text{otherwise} \end{cases} \quad (7)$$

where  $m$  is a strain-rate sensitivity exponent,  $\dot{\gamma}_0$  is a reference strain rate, and  $g^{\alpha}$  is the current flow stress on slip system  $\alpha$ . As noted in the literature [21],

[18], this formulation returns unrealistic slip strain rates for values of  $\tau^\alpha/g^\alpha$  much different than unity. Hence, we use the form of this law presented by Cuitiño and Ortiz [5],

$$\dot{\gamma}^\alpha = \dot{\gamma}_0 \left[ \left( \frac{\tau^\alpha}{g^\alpha} \right)^{\frac{1}{m}} - 1 \right], \tau^\alpha \geq g^\alpha \quad (8)$$

where it is assumed that  $\dot{\gamma}^\alpha = 0$  if  $\tau^\alpha < g^\alpha$ . Note that we have assumed that slip in any system must be positive. That is, the combination of direction  $\bar{\mathbf{s}}^\alpha$  and normal vector  $\bar{\mathbf{m}}^\alpha$  is taken to be a different system than the combination of direction  $-\bar{\mathbf{s}}^\alpha$  and normal vector  $\bar{\mathbf{m}}^\alpha$ . Hence, slip will only occur for  $\tau^\alpha > g^\alpha$ . This modification to the power law representation removes the singularity often seen at  $\tau^\alpha = g^\alpha$ , naturally introducing the result of zero slip velocity when the resolved shear stress and flow stress are equal. The hardening relation governing the value of  $g^\alpha$  is given as

$$\dot{g}^\alpha = \sum_{\beta} h^{\alpha\beta} \dot{\gamma}^\beta \quad (9)$$

where  $h^{\alpha\beta}$  are the hardening moduli. These hardening moduli are provided from a statistical analysis based on the analysis of Ortiz and Popov [24], with the result

$$h^{\alpha\alpha} = h_c(t) \frac{2[\tau^\alpha(t)]^3}{\tau_c^3(t)} \left[ \cosh \left( \frac{\tau_c^2(t)}{[\tau^\alpha(t)]^2} \right) - 1 \right] \quad (10)$$

where

$$\tau_c(t) = a\mu b\sqrt{\pi n^\alpha(t)}, \quad h_c(t) = \frac{\tau_c(t)}{\gamma_c^\alpha(t)} \quad (11)$$

are a characteristic shear stress and plastic modulus,  $a$  is a coefficient (on the order of 0.3),  $b$  is the Burgers vector,  $\mu$  is the shear modulus,  $n(t)$  is the area density of forest dislocations intersecting the slip plane of system  $\alpha$ , and the characteristic strain  $\gamma_c$  is dependent upon the Burgers vector, the dislocation area density in system  $\alpha$ , and the average distance between point obstacles. The off-diagonal (cross-hardening) terms  $h^{\alpha\beta}$ ,  $\alpha \neq \beta$  are taken to be zero. The effect of slip in one system on the hardening characteristics of another is presumed to be described by the forest dislocation density  $n^\alpha$ . Francosi and Zaoui [8] determined interaction parameters  $a^{\alpha\beta}$  describing the dependence of the forest obstacles seen in system  $\alpha$  on the dislocation density in system  $\beta$ ,  $\rho^\beta$ :

$$n^\alpha = \sum_{\beta} a^{\alpha\beta} \rho^\beta \quad (12)$$

These parameters  $a^{\alpha\beta}$  are available for both FCC and BCC crystals [8], [7]. For the case of quasi-static deformation of an FCC crystal, these dimensionless parameters are as follows:

$a_0$	$8 \times 10^{-4}$
$a_1/a_0$	5.7
$a_2/a_0$	10.2
$a_3/a_0$	16.6

Table 1: FCC Interaction Coefficients

## 2.1 Implicit formulation

This constitutive framework was presented in the context of a fully implicit update scheme by Cuitiño and Ortiz. The general update procedure is to presume the unknowns of the deformations are the slip strain rates  $\dot{\gamma}^\alpha$ , and to take as input the updated overall deformation gradient in the undeformed configuration,  $\mathbf{F}_{n+1}$ . This is accomplished by discretizing the viscosity law and solving it for the resolved shear stress  $\tau_{n+1}^\alpha$ ,

$$\tau_{n+1}^\alpha = \psi \left( \frac{\Delta\gamma^\alpha}{\Delta t}, g_{n+1}^\alpha \right) \quad (13)$$

where we note that  $g_{n+1}^\alpha$  is a function of  $\Delta\gamma$ , the vector of all  $\Delta\gamma^\alpha$ , through the hardening law (9). Since we may write

$$\tau^\alpha = (\bar{\mathbf{C}}^e \bar{\mathbf{s}}^\alpha)^T \bar{\mathbf{S}} \bar{\mathbf{m}}^\alpha \quad (14)$$

we find that we can express (13) as a function of the form

$$f^\alpha(\Delta\gamma) = \tau_{n+1}^\alpha - \psi \left( \frac{\Delta\gamma^\alpha}{\Delta t}, g_{n+1}^\alpha \right) = 0 \quad (15)$$

which may be solved using a Newton-Raphson iteration. This is possible because the Jacobian matrix of (15) may be computed explicitly [5], [18]. This implicit approach converges rapidly, within two or three Newton-Raphson iterations.

## 2.2 Explicit formulation

While the implicit formulation exhibits good convergence properties, it (like most implicit integration schemes) is best suited to a larger increment in time. Explicit finite-element simulations (the sort to which we wish to apply our model) inherently use small time integration steps, limited by the time taken for a wave traveling at the Rayleigh speed to cross an element. Hence, an explicit formulation for the update is more appropriate for the application we intend.

The constitutive framework for the explicit form of the model remains untouched. Additionally, the unknowns of the crystal plasticity problem remain unchanged. That is, we design our constitutive update to take  $\mathbf{F}_{n+1}$  as an input, solving for the unknown slip shear rates. Instead of solving iteratively for the ensemble of slip rates, we determine the shear rates in a sequential manner. The evaluation at step  $t_{n+1}$  is based on the hardening information and slip velocities from step  $t_n$ . The explicit procedure used here can be summarized as follows:

1. Calculate  $g^\alpha$ ,  $h^{\alpha\alpha}$  for all systems based on step  $t_n$ .
2. Compute  $\mathbf{F}^e = \mathbf{F}_{n+1}\mathbf{F}_n^p$  and evaluate  $\tau^\alpha$  for all systems.
3. If  $\tau^\alpha < g^\alpha$  for all systems, go to step 6. Otherwise:
4. Apply  $\Delta\mathbf{F}^p = \dot{\gamma}_n^\alpha \Delta t (\bar{\mathbf{s}}^\alpha \otimes \bar{\mathbf{m}}^\alpha)$  due to the unused slip system  $\alpha$  for which  $\tau^\alpha - g^\alpha$  is largest.
5. Premultiply  $\mathbf{F}^p$  by  $\Delta\mathbf{F}^p$ , return to step 2 using this result.
6. Compute new slip rates  $\dot{\gamma}_{n+1}^\alpha$  and hardening moduli  $h^{\alpha\alpha}$ .

Instead of iterating on the ensemble of slip systems, we now activate the system having the largest overstress and repeat until no unused systems exist for which the resolved shear stress exceeds the flow stress from the previous step. We are using the previous step as a predictor for the state during the next step. Logically, then, we expect the quality of the prediction to diminish as we attempt to take longer time steps  $\Delta t$ , which is true. As we will see in Section 3, the time required for an integration approaches that used for a fully elastic step. Depending on the slip activity during step  $t_n$ , the iteration will diverge for values of  $\Delta t$  that are excessively large. Simulations on finite element meshes have shown that this value of  $\Delta t$  may be smaller than the maximum  $\Delta t$  allowed by the mesh. In other words, the maximal time step achieved by such a simulation would depend not upon the chosen mesh, but on the material model. We found this result to be unacceptable, and devised a solution described below.

### 2.3 Subcycling formulation

In order to work around the maximal time step limitation of the explicit model, we first need to understand why the model fails. The crystal plasticity model we have chosen requires that  $\tau^\alpha \geq g^\alpha$  for all active slip systems  $\alpha$ . Further, since the explicit formulation uses the hardening data from step  $t_n$  to predict the slip rates at  $t_{n+1}$ , we may write

$$\tau_{n+1}^\alpha = \tau(\dot{\gamma}_n^\alpha, \Delta t, \mathbf{F}_n^p) \quad (16)$$

That is, the resolved shear stress depends only on the slip increments, the time step, and the plastic deformation gradient at time  $t_n$ . This dependence is manifested through the determination of  $\Delta\mathbf{F}^p$  described in step 4 of the procedure above. The change in the flow stress on a system  $\alpha$  is evaluated as

$$g_{n+1}^\alpha = g_n^\alpha + h_n^{\alpha\alpha} \dot{\gamma}_n^\alpha \Delta t \quad (17)$$

which is linear in  $\Delta t$ . The relation (16) depends only on  $\Delta t$ , albeit nonlinearly. Since we require  $\tau^\alpha \geq g^\alpha$ , we can set (16) equal to (17) and solve iteratively for  $\Delta t_c$ , where we define  $\Delta t_c$  as the maximum (“critical”) time increment for which our constraint is satisfied.

In practice, we do not need the actual value of  $\Delta t_c$  in order to proceed with the integration. We are merely interested in whether we need to invoke the sub-cycling algorithm. If the given  $\Delta t < \Delta t_c$ , the evaluation may proceed without sub-cycling. If  $\Delta t > \Delta t_c$ , sub-cycling is activated. It should be noted that the increments used for the deformation gradient within the sub-cycling procedure must be consistent with the multiplicative decomposition. The integration proceeds by dividing the overall step  $\Delta t$  into smaller increments  $\Delta \tilde{t} = \frac{\Delta t}{n} \leq \Delta t_c$ , where  $n$  is the number of sub-cycles. To summarize, the procedure we use is this:

1. Test the condition  $\tau^\alpha \geq g^\alpha$  for all systems active at time  $t_{n+1}$ . If true, go to step 4.
2. Evaluate the desired  $\Delta \mathbf{F}$ . Bisect the desired time step, test this step applying  $\Delta \mathbf{F}^{inc} = (\Delta \mathbf{F})^{1/2}$ .
3. Repeat until condition in step 1 is satisfied.
4. Exit, returning the number of sub-cycles  $n$ , the time step  $\Delta \tilde{t} = \Delta t/n$ , and the incremental deformation  $(\Delta \mathbf{F})^{1/n}$ .

This procedure has the effect of adding more evaluations of the explicit step for each global step, since the convergence test itself is an explicit evaluation. However, we will see from the relative computational speed of the models that this small net loss of time is converted into a large gain. In general, not every step of a simulation requires the largest amount of sub-cycles to complete. Without sub-cycling, we would be constrained by the *smallest*  $\Delta t_c$  required by any step. The sub-cycling implementation takes advantage of the larger  $\Delta t_c$  values available in most steps. Additionally, for a large-scale simulation, not every quadrature point in the mesh requires sub-cycling at a given time step. It may well be, for a dynamic simulation, that part of the material is highly plastic while another is still in the elastic range. The sub-cycling implementation allows the steps that are easier to evaluate to be finished quickly, without wasting many steps moving through the less computationally-intensive elastic region. In this way, the sub-cycling algorithm is analogous to an adaptive time step that activates only when necessary.

Note that, in actuality, we never solve for the critical time step  $\Delta t_c$ . Instead, we solve for the largest step  $\Delta t/2^n$  such that the condition in step 1 is satisfied. Our chosen method has two useful benefits. First, bisection is nearly trivial to implement and is computationally inexpensive (no derivatives to evaluate, for example). Second, while we do not arrive at the critical time step, we return a time step  $\Delta \tilde{t} \leq \Delta t_c$ . Since  $\Delta t_c$  is the maximum step we can take while maintaining convergence, the method we have chosen provides a built-in error tolerance to the time step evaluation. If we try to solve for  $\Delta t_c$  exactly, we may find that small, unavoidable numerical errors in this solution would cause the integration to fail. The bisection solution helps reduce or eliminate this pitfall, resulting in a more robust crystal plasticity algorithm.

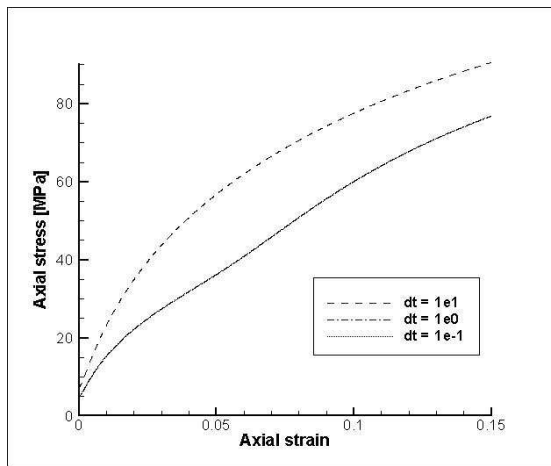


Figure 1: Variations in implicit model results with time step.

### 3 Accuracy of the Algorithm

We will evaluate our explicit model and subcycling implementation in two phases. First, we will compare the results from the implicit model to the explicit, with the goal of proving that the computational speed we gain does not come at too steep of a price in accuracy. Then, we will apply the algorithm to some larger-scale simulations, highlighting the increase in processing speed seen in using the subcycling algorithm.

An important consideration in comparing the results from the implicit and explicit algorithms is time-convergence (stationarity) of the results, especially for the implicit model. Most numerical integrations exhibit some form of time-step dependency; Figure 1 illustrates the dependency for several simulations of the quasi-static deformation of a copper crystal in tension along the [112] crystal axis. If we choose a time step  $\Delta t = 10$ , the model predicts a different response than  $\Delta t = 1$  or  $\Delta t = 0.1$ . Note that the predicted responses for the latter two time steps differ by 0.008% of the smaller value. If we require our model responses to be stationary for smaller time steps, then we should use  $\Delta t$  of no larger than 1. Since we wish to apply our models to dynamic finite-element simulations using very small time steps, i.e.,  $O(10^{-8})$ , stationarity of the results with respect to the time step is a necessary condition. The results presented here match well with experimental data [8]; we list the model parameters used in Table 2.

Figure 2 is of the same form as Figure 1, but for the explicit model. The time-converged step is around  $\Delta t = 10^{-4}$ , while the results at  $\Delta t = 10^{-3}$  are shown to be vastly different.



Elastic Constant $C_{11}$	168.4 GPa
Elastic Constant $C_{12}$	121.4 GPa
Elastic Constant $C_{44}$	75.4 GPa
$g_0$	2.0 MPa
$\dot{\gamma}_0$	10 sec <sup>-1</sup>
$m$	0.1
$a$ [see Eq. (11)]	0.3
$b$	$2.56 \times 10^{-10}$
Initial dislocation density, $\rho_0$	$10^{12} m^{-2}$
Saturation dislocation density, $\rho_{sat}$	$10^{15} m^{-2}$
Saturation strain, $\gamma_{sat}$	0.5%

Table 2: Definition of Symbols

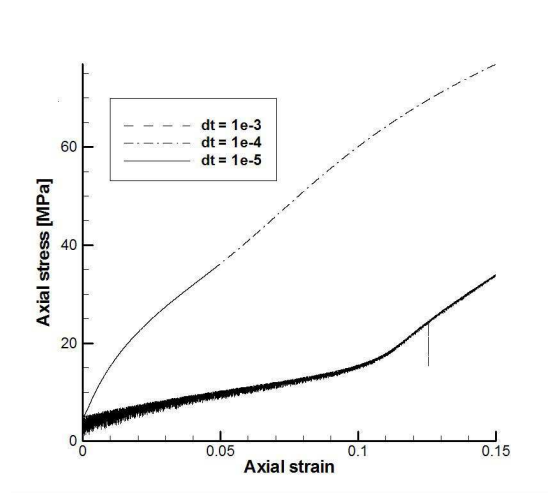


Figure 2: Time-convergence behavior of the explicit model.

Our next step is to show that the explicit model with subcycling gives results similar to the explicit model without subcycling. In order to illustrate this part, we applied the implicit model and explicit model with and without subcycling to a single-integration-point simulation of a rolling test. The crystal is compressed at high strain rate ( $\sim 5000/s$ ) along its  $[001]$  axis, with the global  $X - Y$  axes at  $45^\circ$  to the crystal  $x - y$  axes. The global  $Y$  face is constrained. We choose this sort of test for two reasons: First, this test is closer to the type of simulation we wish to perform with the explicit model. Second, we do not wish for the constitutive tangents to cloud the results, since we intend to apply our subcycling algorithm to simulations not requiring the constitutive tangents. Figures 3-6 show the time-convergence behavior for the implicit, explicit and subcycling models. Figure 7 compares the results for a time-converged implicit and explicit model to results that include the use of subcycling ( $\Delta t \sim 10^{-8}$ ). The difference among the models at 15% reduction is 0.08% of the smallest value (in this case, the implicit). If we take a smaller time step with the subcycling model, the  $\Delta t_c$  constraint is not violated and the subcycling model becomes the explicit model exactly. While we see oscillations in the force-deformation response when we apply subcycling, these oscillations are in general about the converged solution. As expected, the subcycling formulation continually over- and under-predicts the stress response, eventually settling on the correct value. We gain about an order of magnitude in the time step using subcycling. If we attempt to take a larger step than what is depicted, we find that the simulation no longer converges at a very early point in the deformation (within the first 50 steps).

A closer analysis of the output shows that the subcycling tests that failed had large oscillations in the stress-strain curve, as demonstrated by the simulation using  $\Delta t = 10^{-8}$ . This manner of failure is due to the issue of time-convergence. If the original input time step  $\Delta t$  is greater than the converged time step, then steps that involve subcycling will be on a time-converged solution curve, while any steps that do not involve subcycling may not be on the time-converged curve. The overall solution, then, runs on two paths; this condition eventually causes the overall solution to diverge.

While these oscillations are a concern at the integration-point level, this effect tends to diminish within the framework of a large-scale finite-element solution. For such simulations, the subcycling implementation acts to make the system more robust. This is because of the necessarily smaller time steps used in the finite-element solution. These smaller time steps are more likely to be converged<sup>1</sup>. The difference between the subcycling path and the smoother path without subcycling will be less dramatic. Another important point from this analysis is that the subcycling algorithm used here does not increase the effective time step over which the model can progress without bound. There are two reasons for this. The first is numerical precision; that is, the  $\Delta \mathbf{F}^{\frac{1}{2}}$  calculations lead to matrices that approach the identity as  $n \rightarrow \infty$ . For steps

---

<sup>1</sup>Certainly, the smaller time step is closer to the converged step than the single-integration-point steps above

of smaller than about  $10^{-15}$ , the difference between 1 and  $(1 + \varepsilon)$  is no longer computationally resolved. Hence, if we try to take steps smaller than this, the  $\Delta\mathbf{F}$  matrix will be seen by the machine as the identity. Secondly, our subcycling algorithm uses an estimate over the entire desired time step before taking the first step. This estimate will be good so long as the velocity in every slip system ( $\dot{\gamma}^\alpha$ ) decreases across the number of cycles. If we activate new systems in a subcycle, or if the velocity in a previously activated system exceeds the initial estimate, we are no longer guaranteed that the model will converge. It may be argued, then, that the current subcycling algorithm should be modified to be recursive, testing both the initial time step and that of each subcycle. The present formulation, however, has proven to be sufficient; the benefit gained by introducing a recursive subcycling algorithm may well be outweighed by the effort required in its implementation, both in terms of programming and computation time.

We close our discussion of the constitutive-level results with comparisons of the computational time between the implicit and explicit integration. Figure 8 presents the variation of computation time for one integration point versus deformation for the rolling-type test used above. (We omit the times for the subcycling model since the core of the integration is the explicit model.) We obtained these curves by running each update over the same set of parameters 50 times and averaging the processor time used for the full set. These results show that the explicit calculation is about five to six times faster than the implicit. While by no means dramatic, this gain of time is significant; an implicit simulation lasting a week would (at the same strain step) take about a day for the explicit model to complete. Even for the constitutive-level analysis in this section, we can see the interplay between the largest stationary time step and the compute speed. The tensile tests (Figures 1 and 2) at low strain rate allow the implicit model to take a step four orders of magnitude longer than the explicit, more than counteracting the half order of magnitude of compute speed gained by the explicit model. However, the rolling-type tests presented above require the implicit model to take a time step on the order of  $\Delta t = 10^{-10}$  and the explicit model<sup>2</sup> to take a time step on the order of  $\Delta t = 10^{-9}$ . In this case, the explicit model is simply faster, by an overall factor of about 50.

## 4 Large-Scale Simulation Results

The motivation for our foregoing discussion was the application of the derived material models to large-scale simulations requiring many integrations over small time steps. Here we provide a few examples of such tests performed using these algorithms.

---

<sup>2</sup>Without subcycling.

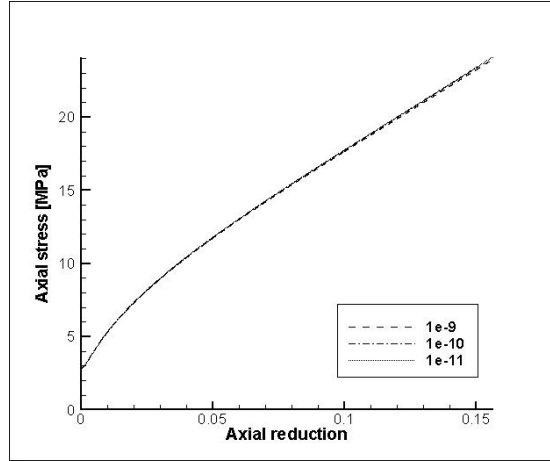


Figure 3: High-rate test using the implicit formulation. The results using  $\Delta t = 10^{-10}$  and  $\Delta t = 10^{-11}$  differ by 0.06% at 15% reduction.

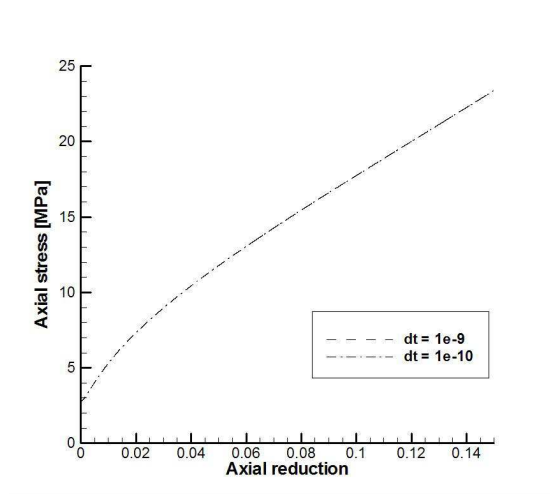


Figure 4: Time stationarity test for compressive deformation using the explicit model. The two curves here differ by 0.0009% at 15% reduction.

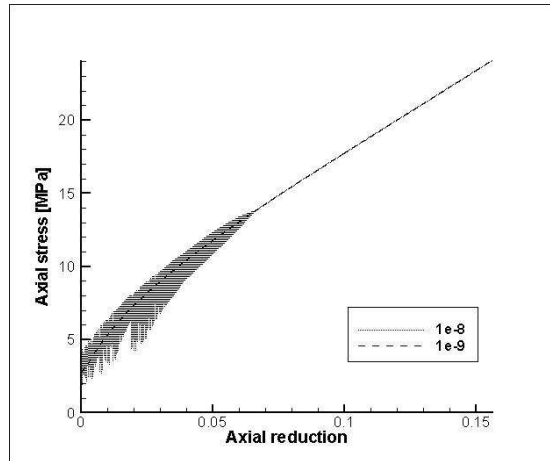


Figure 5: Convergence test using subcycling. After the initial oscillations, the curves shown here are exactly atop one another.

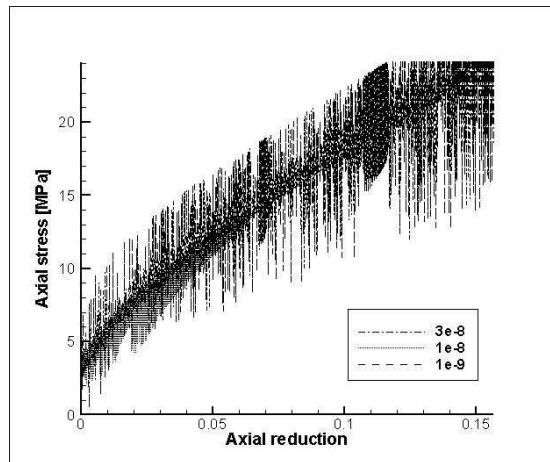


Figure 6: Showing the larger-scale oscillations introduced in the subcycling response for increased time steps. Larger steps than  $\Delta t = 3 \times 10^{-8}$  diverge.

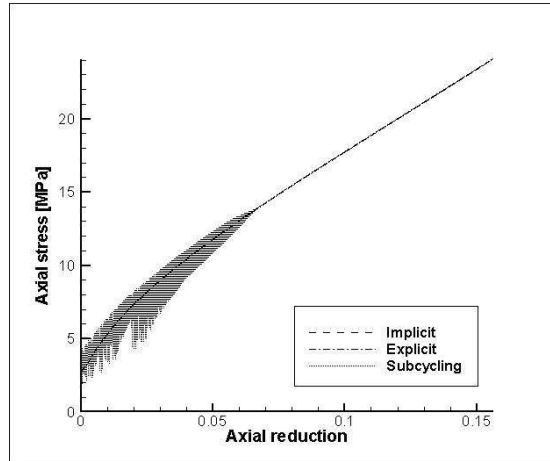


Figure 7: Converged curves for implicit, explicit and subcycling models.

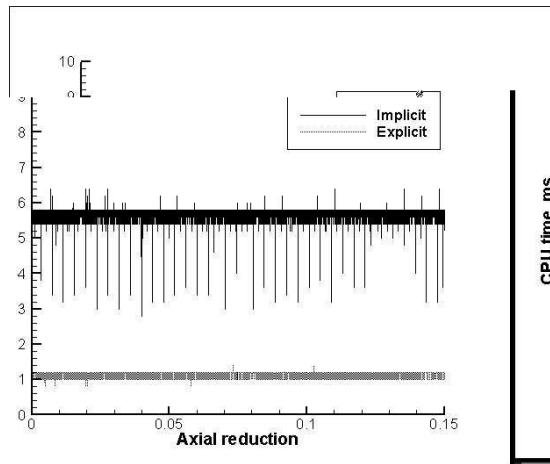


Figure 8: Comparison between compute times per second for the implicit and explicit update formulations.

## 4.1 Rolling Test of FCC Aluminum

We begin with a 1 mm aluminum cube oriented such that the crystal  $z$  axis lies on the global  $Z$  axis, and the other two axes defined by a  $45^\circ$  rotation about the crystal  $z$  axis. This cube is subjected to a strain rate of  $\sim 5000/s$  along the global  $Z$  axis. The cube is constrained so that expansion in the global  $Y$  direction is not possible, but it may deform freely in all other directions. The results below show the force applied versus the net reduction, and the initial and final textures. The qualitative behavior of the force-deformation curve agrees with the physical interpretation of the simulation. The simulation captures the fluctuations in the applied force due to wave reflection from the opposite face of the cube, which are eventually damped out. To help make the case for our subcycling algorithm, we present results for the explicit model both with and without our subcycling algorithm.

The effects of adding subcycling to the explicit model are striking. We will use an integration over a tetrahedral mesh of a cubic sample, modeling one grain in each direction (initial shape given in Figure 9) deformed in a rolling experiment as a sample case. Without the addition of subcycling, a simulation using the explicit integration model described above for an FCC material would require eight hours before the thickness reaches 50% reduction, using eight processors. This is not due to a limitation of the mesh, but rather of the material model; the material model is found to require a stable time step of about 25% that required by the tetrahedron geometry. If we try the identical simulation using the subcycling algorithm described above, we find that the maximum stable time step becomes that of the mesh - the material model is no longer the limiting factor. As a result, this same simulation on the same eight processors requires about fifteen minutes to reach 50% reduction. The gain of time is nonlinear because not all quadrature points require subcycling at any one time. It may be that only one of the approximately 380 integration points requires a smaller step at a given time. Without a subcycling algorithm, that one integration point would be enough to require the time step for the entire mesh to be reduced by a factor of four or more.

Figure 10 compares the force-reduction curves for three simulations. The difference among these simulations is the maximum allowed time step. The `time_factor` variable in the plot legend is a premultiplying factor applied to the mesh stable time step. The simulation using `time_factor` 0.1 required no subcycling to complete. At first glance, it seems that the simulation without subcycling is capturing more of the reflected waves than the one using subcycling at the beginning of the deformation. However, if we look at a close-up of this region, we find that the simulations cross the same points where they exist; Figure 11. That is, we are capturing the same curve with varying levels of detail. This implies that the additional oscillations seen for `time_factor=0.1` are a result of having a smaller time step, and not a failing of the subcycling implementation.

We also attempted a simulation of this deformation using our implicit formulation. The force-deformation results are shown in Figure 12 and 13, compared

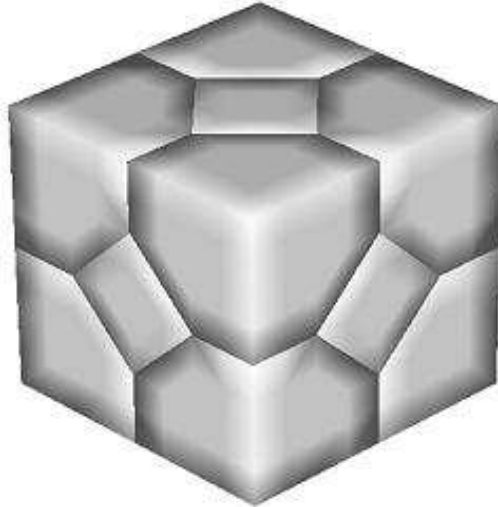


Figure 9: Initial cube for the tests that follow. This cube is meshed with 384 tetrahedra. The heavy lines denote boundaries between twenty-sided polyhedral grains.

to the explicit formulation at `time_factor` of 0.5. (Note that the implicit model was capable of stepping as large as `time_factor` 0.75, but the results at this time step are not stationary as defined above). We plot the time taken by each model versus the time step in Figure 17. Interestingly, we start to see a negative return when we increase the time step past 75% of the mesh time. This is due to the larger number of subcycles required for the full mesh time step to proceed. The number of extra evaluations required outweighs the 33% larger time step for this case. In fact, the simulation with `time_factor`=1.0 required almost as much time to complete as that with `time_factor`=0.5. Thus, blindly increasing the time step up to the value allowed by the mesh does not necessarily produce the most efficient simulation. Note also that the implicit model is slower at every time step by about a factor of 5; this coincides nicely with the predictions of Figure 8.

Another way in which we can check our subcycling implementation is by examining the predicted material texture at the end of the deformation. Each of our rolling tests was given the initial texture in Figure 14. Figure 15 shows that we recover similar  $\langle 111 \rangle$  textures for all the explicit simulations, given the same initial textures. Also, the implicit model predicts similar textures to the explicit for the same time step; see Figure .These textures agree well with measured textures from the literature. In order to produce these textures, we reduced the interaction parameter  $a_0$  to  $2 \times 10^{-5}$  (see Table 1). Figure 16 shows the final textures obtained from implicit model simulations, using time steps at



50% and 10% of the mesh value. These textures are similar to those predicted by the explicit model.

Note that the predicted forces in the foregoing figures are quite small, on the order of 10 N. Since this force is applied to a 1 mm cube, this translates directly to 10 MPa. The low force values returned are due to our rather small choice of viscosity exponent ( $m = 0.1$ ). This exponent gives very good force matching for the quasi-static cases above, but it does not reflect the physics of the dynamic simulations very well. This viscosity exponent was chosen for these simulations to test the limitations of our explicit model. High-viscosity deformations will have lower rates, thus less plasticity and hardening, and therefore will easily converge for larger times (i.e.,  $\Delta t_c$  will increase with the viscosity exponent). By taking on the more challenging rate-independent limit, we can be sure our model will perform well in the somewhat easier high-viscosity simulations. To demonstrate this, we present Figure 18, which shows results for time\_factors of 1.0 and 0.75 with the viscosity exponent changed to 1.0. The forces increase significantly from what we saw in the rate-independent limit; now, our forces imply stresses in the range of several GPa. Interestingly, the simulation using the full time step was 25% (6 minutes) faster than the simulation with 75% of the mesh step for this set of parameters. Since the larger viscosity exponent leads to less plasticity and therefore less hardening, it follows that the  $\Delta t_c$  values for these simulations are longer, reducing the number of subcycles needed to converge. Figure 19 shows the texture for the case with time\_factor=1.0; our agreement with measured values degrades. In fact, we detect no texture evolution whatsoever, since the amount of plastic deformation has reduced considerably due to the increased viscosity exponent. This question, unfortunately, cannot be resolved at the present time. The published texture data is measured after the completed deformation, after a period of time long enough to allow the deformed sample to relax. Presumably, the texture evolution continues after the test is completed. A more accurate comparison would be drawn between the current results and *in situ* texture evolution data. The appropriate set of model parameters may then be determined.

## 4.2 Polycrystal tests

We have also performed some simulations of polycrystals under similar conditions. We have used both Taylor averaging and direct numerical simulation (DNS) to model the polycrystalline behavior based on the single-crystal model. A discussion of the merits and drawbacks of these approaches has been discussed elsewhere (see Zhao, *et al* [31]). We provide some of the results of these simulations here as they pertain to the explicit constitutive update scheme, with and without subcycling.

We noted above the large fluctuations in force-deformation response for a single integration point using the subcycling implementation. These oscillations had little effect on the overall results for single crystals; presumably their effects were damped out by the overall bulk of the available quadrature points. However, we find that these fluctuations are important for modeling of polycrystals.

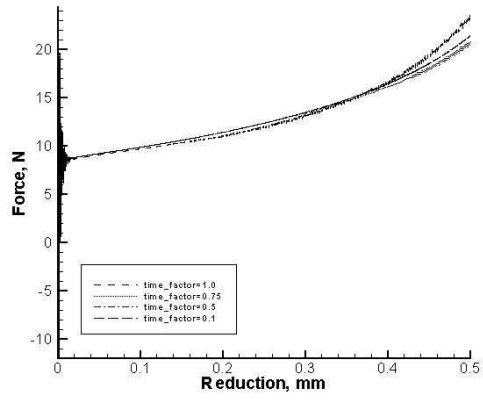


Figure 10: Comparison of force-deformation curves for explicit model runs with several different time steps.

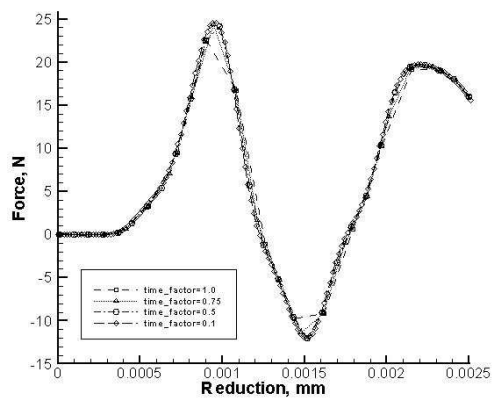


Figure 11: Close-up of the foregoing figure, with symbols designating points returned.

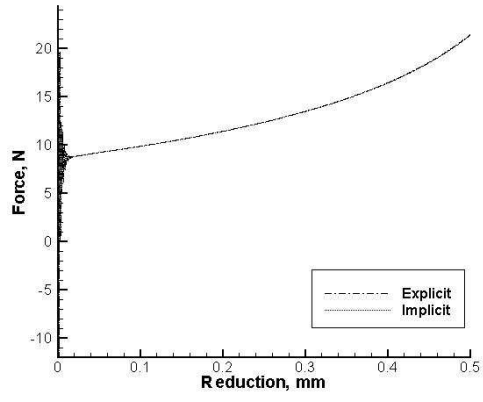


Figure 12: Force response predictions for the explicit and implicit model, both using 50% of the maximal mesh time step.

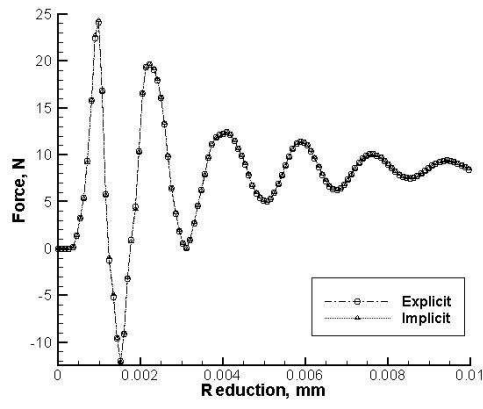


Figure 13: Close-up of the implicit and explicit force curves. Note that the symbols lie atop one another.

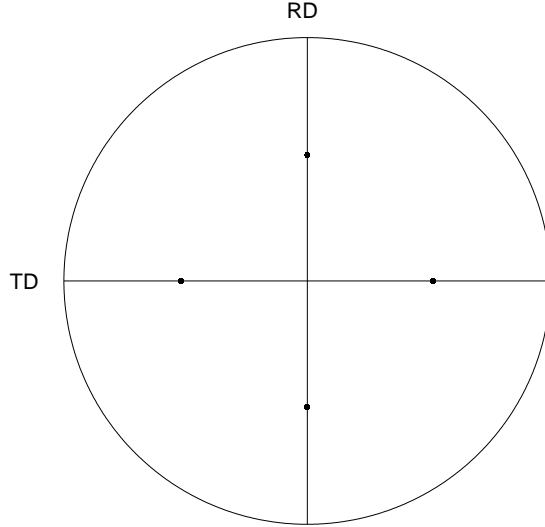


Figure 14: Initial  $\langle 111 \rangle$  texture for the tests in this section.

Specifically, we tested a sample using the same mesh as the above, but applied the deformation to a polycrystal having 91 orientations using a Taylor averaging approach; that is, we presume the overall deformation gradient and deformation rate are the same for all orientations, and average to find the resulting stress. Where the subcycling approach allowed our simulations to use the 100% of the time step allowable by the mesh for a single crystal (i.e.,  $\text{time\_factor}=0.75$ ), we were forced to reduce to a time step at 25% of that required by the mesh for this polycrystal. Simulations applying DNS show similar behavior. We feel the difficulty is a product of the interfaces of the polycrystalline grains. Instead of having only a gradient between the part of the crystal that is heavily deformed and the portion that is still nearly elastic (as in the single-crystal case), the polycrystal introduces gradients between parts of the crystal that have similar overall deformation gradients and yet different plastic behavior. It stands to reason that neighboring points in a polycrystalline mesh may well require vastly different numbers of subcycles to meet the  $\Delta t_c$  constraint. At points such as this, one element will then be on the more stable converged path, while another is on the somewhat volatile subcycling path. The result is that subcycling loses some of its effectiveness for polycrystal modeling.

Subcycling still benefits the modeling effort, however. Instead of being forced to a small step of 10% the overall mesh step, we can still increase our time step by a factor of 2.5. The results for averaging 91 orientations took about four days, which is a linear scaling from the time taken by a single orientation at the same time step. The results are shown below; the force results in Figure 20, and the final texture in Figure 21.

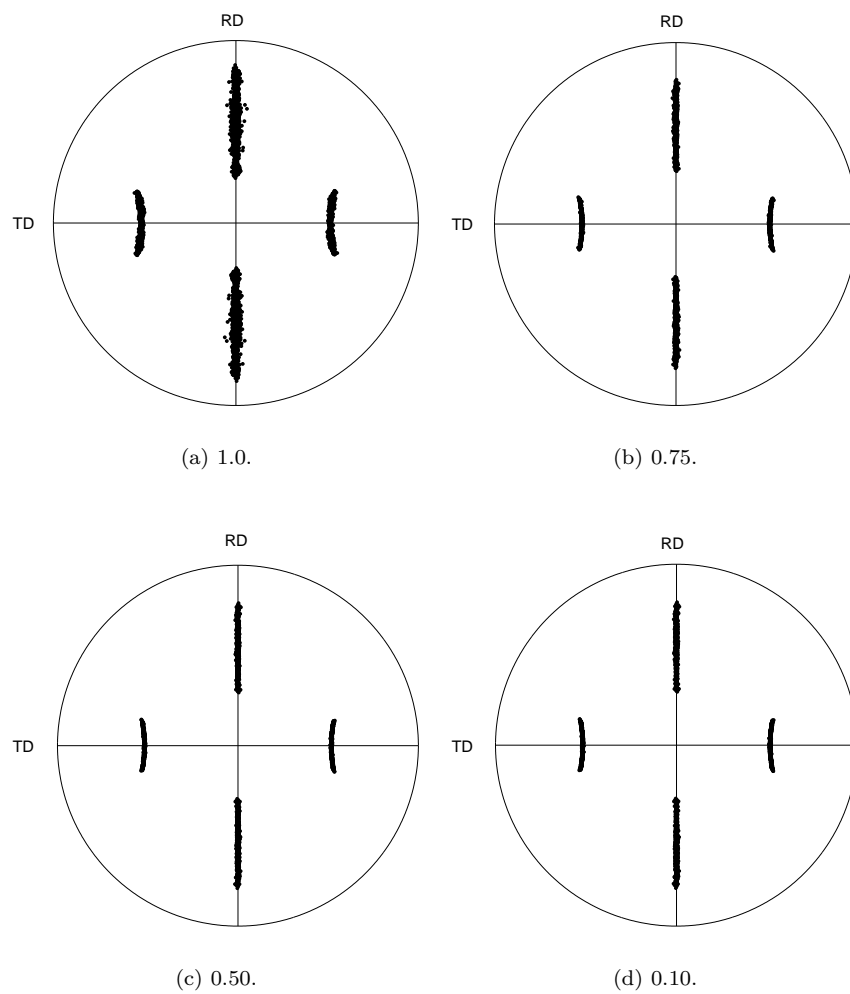


Figure 15: Final textures for the explicit model simulations for different time factors.

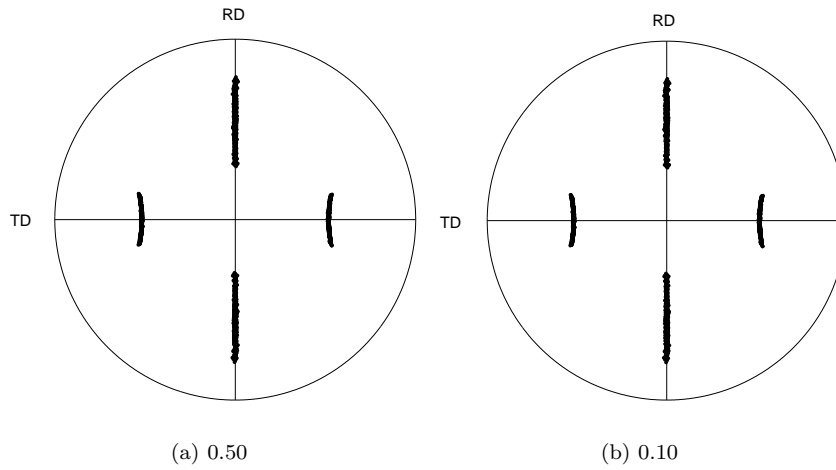


Figure 16: Textures predicted by the implicit model simulations for different time factors.

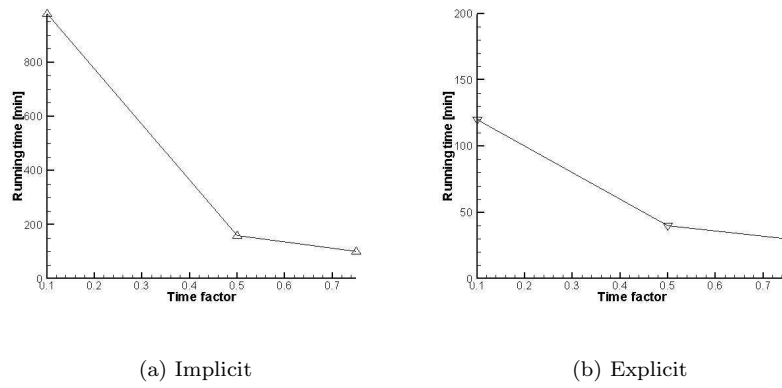


Figure 17: Comparison of running time versus time step for both implicit and explicit models.

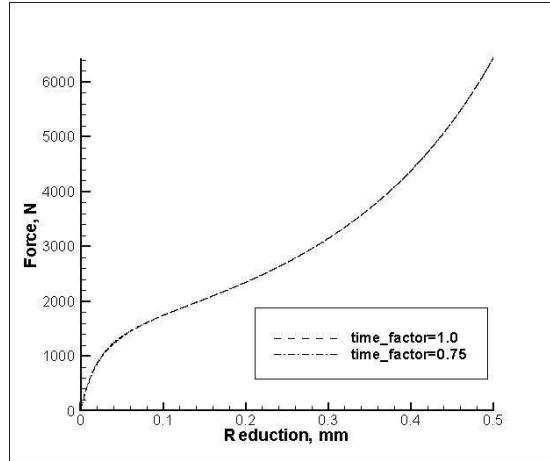


Figure 18: Force-deformation curves for two simulations using viscosity exponent  $m = 1.0$ .

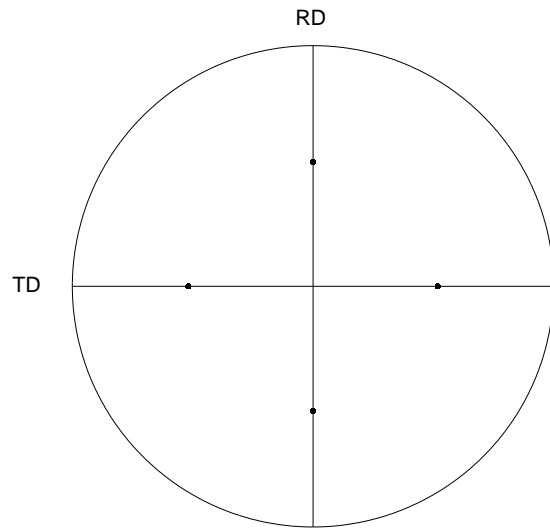


Figure 19: Texture prediction for the high-viscosity simulation.

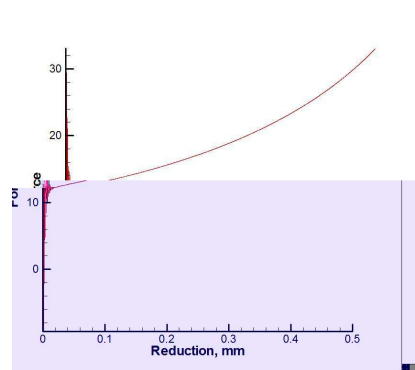


Figure 20: Predicted force-deformation curve for the polycrystal sample.

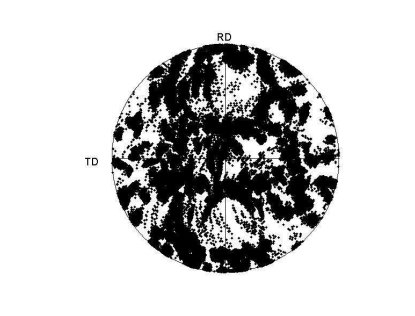


Figure 21: Predicted texture for Taylor averaging simulation using 91 orientations per integration point.



## 5 Conclusions

We have demonstrated two model improvements which enhance the computational speed of an implicit constitutive update, in cases dominated by the global time step. Beginning with an implicit formulation based on the model of Cuitiño and Ortiz, we modified the update to an explicit formulation. This explicit formulation was shown to be five to six times faster than the original implicit algorithm per update step at the constitutive level, without loss of accuracy. The explicit update is limited by the size of time step that can be taken. We were able to increase this maximal time step by an order of magnitude for single crystals by introducing a subcycling algorithm to the explicit form. All three models produce the same stress-strain behavior at the integration point level for the same input parameters.

We then applied our three update formulations to large-scale finite-element calculations. The explicit update with subcycling was shown to be able to integrate a larger time step for single crystals than even the implicit, since the subcycling procedure changes the larger input time step into several smaller steps that can be evaluated by our explicit algorithm. For polycrystals, the subcycling algorithm does not allow simulations to run at the full mesh time step. However, the subcycling implementation allows an increase in the maximum time step over the explicit model without subcycling, and so results in an improvement in computational speed.

Notably, the implicit and explicit models each have their uses. The implicit model is best suited to quasi-static simulations allowing larger time steps to be used<sup>3</sup>. In this sort of simulation, the gain of time per step realized by the explicit model is countered by the number of subcycles necessary to use the explicit model. Dynamic simulations, for which the time step is typically very short, are well-suited to the explicit model's capabilities. For such simulations, the explicit model proves a robust algorithm.

## Acknowledgements

This work is sponsored by the U.S. Department of Energy's Accelerated Strategic Computing Initiative (ASC) and the ASC Center at the California Institute of Technology.

## References

- [1] R. Asaro. Micromechanics of crystals and polycrystals. *Advances in Applied Mechanics*, 23:1–115, 1983.
- [2] R. Asaro and J. Rice. Strain localization in ductile single crystals. *Journal of the Mechanics and Physics of Solids*, 25:309–338, 1977.

---

<sup>3</sup>Limited, of course, by the converged time step

- [3] J. Bassani. Plastic flow of crystals. *Advances in Applied Mechanics*, 30:192–258, 1993.
- [4] J. Bishop and R. Hill. A theoretical derivation of the plastic properties of a polycrystalline center-faced metal. *Philosophical Magazine*, 42:414–427, 1951.
- [5] A. Cuitiño and M. Ortiz. Computational modeling of single crystals. *Modelling and Simulation in Materials Science and Engineering*, 1:255–263, 1993.
- [6] Y. Dafalias. Corotational rates of kinematic hardening at large plastic deformation. *Journal of Applied Mechanics*, 50:561, 1983.
- [7] P. Francosi. Glide mechanisms in bcc crystals and investigation of the case of  $\alpha$ -iron through multislip and latent hardening tests. *Acta Metallurgica*, 33:1601, 1983.
- [8] P. Francosi and A. Zaoui. Multislip in fcc crystals: A theoretical approach compared with experimental data. *Acta Metallurgica*, 30:1627, 1982.
- [9] A. Green and P. Naghdi. Some remarks on elastic-plastic deformation at finite strain. *International Journal of Engineering Science*, 9:1219–1229, 1971.
- [10] K. Havner. On the mechanics of crystalline solids. *Journal of the Mechanics and Physics of Solids*, 21:383, 1973.
- [11] K. Havner. *Finite Plastic Deformation of Crystalline Solids*. Cambridge University Press, 1992.
- [12] R. Hill. Generalized constitutive relations for incremental deformation of metal crystals by multislips. *Journal of the Mechanics and Physics of Solids*, 14:95–102, 1966.
- [13] J. Hutchinson. Bounds and self-consistent estimates for creep of polycrystalline materials. *Proceedings of the Royal Society of London*, A348:101–127, 1976.
- [14] U. Kocks, C. Tomé, and H. Wenk. *Texture and Anisotropy: Preferred Orientations in Polycrystals and Their Effect on Material Properties*. Cambridge University Press, 1998.
- [15] J. Kratochvil. Finite-strain theory of crystalline elastic-inelastic materials. *Journal of Applied Physics*, 42:1104–1108, 1971.
- [16] E. Lee. Elastic-plastic deformation at high strains. *Journal of Applied Mechanics*, 36:1–6, 1969.
- [17] E. Lee and D. Liu. Finite strain elastic-plastic theory with application to plane wave analysis. *Journal of Applied Physics*, 38:391–408, 1967.

- [18] X. Ling, M. Horstemeyer, and G. Potirniche. On the numerical implementation of 3d rate dependent single crystal plasticity formulations. *International Journal for Numerical Methods in Engineering*, In review, 2004.
- [19] B. Lorent. On the effects of plastic rotation in the finite deformation of anisotropic elastoplastic materials. *Mechanics of Materials*, 2:287–304, 1983.
- [20] J. Mandel. Plasticité classique et viscoplasticité. *Courses and Lectures, No. 97, ICMS, Udine*, 1971.
- [21] R. McGinty. *Multiscale Representation of Polycrystalline Plasticity*. PhD thesis, Georgia Institute of Technology, 2001.
- [22] S. Nemat-Nasser. Decomposition of strain measures and their rates in finite deformation elastoplasticity. *International Journal of Solids and Structures*, 15:155, 1979.
- [23] E. Onat. Representation of inelastic behavior in the presence of anisotropy and of finite deformations, 1982.
- [24] M. Ortiz and E. Popov. A statistical theory of polycrystalline plasticity. *Computer Methods in Applied Mechanics and Engineering*, 90:781, 1982.
- [25] D. Peirce, R. Asaro, and A. Needleman. An analysis of nonuniform and localized deformation in ductile single crystals. *Acta Metallurgica*, 30:1087–1119, 1982.
- [26] J. Rice. Inelastic constitutive relations for solids: An internal-variable theory and its application to metal plasticity. *Journal of the Mechanics and Physics of Solids*, 19:433, 1971.
- [27] E. Schmid. *Proceedings of the International Congress on Applied Mechanics (Delft)*, page 342, 1924.
- [28] G. Taylor. Plastic strain in metals. *Journal of the Institute of Metals*, 62:307, 1938.
- [29] G. Taylor and C. Elam. The distortion of an aluminum crystal during a tensile test. *Proceedings of the Royal Society of London*, A102:643–667, 1923.
- [30] C. Teodosiu. *Elastic Models of Crystal Defects*. Springer-Verlag, 1982.
- [31] Z. Zhao, S. Kuchnicki, A. Cuitiño, and R. Radovitzky. A comparison of direct numerical simulation and taylor averaging in modeling polycrystalline metals. *Submitted for Review*, 2004.